Theoretical Calculations of Mechanical, Electronic, and Chemical Bonding in CaN_2, SrN_2, and BaN_2

Li-Qin Zhang[a,b], Yan Cheng[a], Zhen-Wei Niu[a], Chang-Ge Piao[a], and Guang-Fu Ji[c]

[a] College of Physical Science and Technology, Sichuan University, Chengdu 610064, China
[b] Department of Physics and Electronic Information, Huaibei Normal University, Huaibei 235000, China
[c] National Key Laboratory for Shock Wave and Detonation Physics Research, Institute of Fluid Physics, Chinese Academy of Engineering Physics, Mianyang 621900, China

Reprint requests to Y. C.; E-mail: ycheng@scu.edu.cn

Z. Naturforsch. **69a**, 619 – 628 (2014) / DOI: 10.5560/ZNA.2014-0062
Received January 3, 2014 / revised May 8, 2014 / published online November 5, 2014

We present a first-principles density functional theory-based study about the impact of pressure on the structural and elastic properties of bulk CaN_2, SrN_2, and BaN_2. Non-spin and spin polarized calculations indicate that the non-spin polarized ground state was more favourable with magnetic moments of 1.049 μ_B, 1.059 μ_B, and 1.014 μ_B for CaN_2, SrN_2, and BaN_2, respectively, and these were in good agreement with previous experimental and theoretical data. The high bulk modulus of CaN_2, SrN_2, and BaN_2 confirm that those compounds have low compressibility and high hardness. The obtained bulk modulus, N–N bond length, and optimized structure parameters are similar to those from previous studies. With an increase in applied pressure the independent elastic constants of CaN_2, SrN_2, and BaN_2 indicated the presence of mechanical instability at 20, 15, and 10 GPa, which is possibly related to phase transitions in addition to a decrease in N–N bond length.

Key words: Density Functional Theory; Elastic Constants; Electronic Structure; Alkaline Earth Diazenides.

1. Introduction

Metal pernitrides MN_2 have been either predicted or directly synthesized and have had a remarkable impact on solid-state and materials chemistry. These compounds contain metal atoms such as osmium, iridium, platinum or alkaline earths together with N_2 pernitride units as complex counter-anions. Binary metal–nitrogen compounds currently play an important role in the most exciting technological applications of materials science. Furthermore, it has been shown that a large bulk modulus and low compressibility are characteristic of iridium nitride [1]. Platinum nitride and titanium nitride have been shown to possess excellent strength and durability [2]. These materials include PtN_2, IrN_2, OsN_2, and PdN_2, and they can be used in optoelectronic devices, sensitive magnetometers, and other metrological equipment [3 – 11]. Kulkarni et al. [9] have identified locally ergodic regions for binary pernitride MN_2 compounds (M = Ca, Sr, Ba, La, and Ti) and have subsequently explored local minima through local optimizations using global optimization techniques.

The first members of these novel nitrogen-rich alkaline earth compounds $M_{AE}N_2$ were discovered and structurally characterized by Kniep et al., thus revealing dinitrogen anions $[N_2]^{2-}$ with N=N double bonds. In 2001, SrN_2, and BaN_2 were synthesized from their corresponding metals at 620 °C under nitrogen pressure in a specialized autoclave system [12 – 14]. Since then noble metal dinitrogen with analogous formulae such as OsN_2, IrN_2, PdN_2, and PtN_2 have been synthesized in laser-heated diamond anvil cells in combination with cryogenically loaded nitrogen at high pressure and temperature [15 – 22]. Experimental results and theoretical predictions of noble-metal pernitrides such as IrN_2, OsN_2, PtN_2, and PdN_2 have shown that they are mechanically hard materials with a hardness exceeding those of noble metals. Recently, alkaline earth diazenides CaN_2, SrN_2, and BaN_2 have been synthesized by the controlled decomposition of their corresponding azides in a multianvil press at high pressure and temperature [23].

However, many basic physical properties of noble metal and alkaline earth diazenides are unknown.

Therefore, in this report we focus on the structural, elastic, electronic, and mechanical stability of SrN_2, BaN_2, and CaN_2 under pressure using the norm-conserving technique together with first principles. The paper is organized as follows: the theoretical method is introduced and the computation details are given in Section 2 upon which the results and discussion are presented in Section 3. Finally, a summary of our work is given in Section 4.

2. Theoretical Method and Computation Details

2.1. Total Energy Electronic Structure Calculations

We used the plane-wave pseudopotential density functional theory method as implemented in the Cambridge serial total energy package (CASTEP) [24]. For electronic structure calculations we used norm-conserving (NC), on-the-fly (OTF), and Vanderbilt ultrasoft pseudopotentials (US) for the interactions of electrons with ion cores. These were used together with the local density approximation (LDA), as proposed by Vosko et al. [25] in the Ceperley–Alder parameterized scheme by Perdew and Zunger (CA-PZ), and the generalized gradient approximation (GGA) proposed by Perdew et al. [26] in the Perdew–Burke–Ernzerhof scheme to describe the exchange and correlation potentials. Pseudo-atomic calculations are performed for Ca $3p^6 4s^2$, Sr $4p^6 5s^2$, Ba $5p^6 6s^2$, and N $2s^2 p^3$. The plane-wave cutoff energies for CaN_2, SrN_2, and BaN_2 were 800 eV, 800 eV, and 900 eV, respectively. Brillouin-zone integration was performed using $9\times9\times9$ grids with the Monkorst–Pack method for pernitride structure optimization [27]. This set of parameters ensured a maximum force of 0.01 eV/Å, a maximum stress of 0.02 GPa, and a maximum displacement of 5.0×10^{-4} Å.

The pressure–volume relationship can be obtained by fitting the calculated energy–volume (E–V) data to the Vinet equation of state (EOS) [28]

$$\ln\left[\frac{Px^2}{3(1-x)}\right] = \ln B_0 + a(1-x)\,,\quad x = \left(\frac{V}{V_0}\right)^{1/3}, \tag{1}$$

where $V = V(0,T)$ is the zero-pressure equilibrium volume, derived by integration of the thermodynamic definition of the thermal expansion coefficient $\alpha(T) = V^{-1}\partial V/\partial T$, that is

$$V(0,T) = V(0,0)\exp\int_0^T \alpha(T)\,\mathrm{d}T, \tag{2}$$

B_0 and a $(= 3(B_0' - 1)/2)$ are the fitting parameters. $B_T(P,T)$ and $B_T'(P,T)$ are given by

$$B_T = -x^2 B_0\,\mathrm{e}^{\alpha(1-x)} f(x), \tag{3}$$

$$B_T' = \left(\frac{\partial B_T}{\partial P}\right)_T = \frac{1}{3}\left[(ax+2) - x\frac{f'(x)}{f(x)}\right], \tag{4}$$

where $f(x) = x - 2 - ax(1-x)$.

2.2. Elastic Properties

To calculate the elastic constants under hydrostatic pressure P, we use the symmetry-dependent strains that are non-volume conserving. The elastic constants C_{ijkl} with respect to the finite strain variables are defined as [29, 30]

$$C_{ijkl} = \left(\frac{\partial\sigma_{ij}(x)}{\partial e_{kl}}\right)_X, \tag{5}$$

where σ_{ij} and e_{kl} are the applied stress and Eulerian strain tensors, and X, x are the coordinates before and after deformation, respectively. Under the hydrostatic pressure P, we have

$$C_{ijkl} = c_{ijkl} + \frac{p}{2}(2\delta_{ij}\delta_{kl} - \delta_{il}\delta_{jk} - \delta_{ik}\delta_{jl}), \tag{6}$$

where c_{ijkl} denote the second-order derivatives with respect to the infinitesimal strain (Eulerian), δ is the finite strain variable. The fourth-rank tensor C generally greatly reduces when taking into account the symmetry of the crystal. From the calculated elastic constants, we can get the mechanical parameters, namely the bulk, shear, and Young's modulus, which are taken as [31–33]:

$$\begin{aligned}
B_{\mathrm{Hill}} &= \frac{1}{2}\left(B_{\mathrm{Reuss}} + B_{\mathrm{Voigt}}\right),\\
B_{\mathrm{Reuss}} &= \left[(2S_{11}+S_{33}) + 2(S_{12}+S_{13})\right]^{-1},\\
B_{\mathrm{Voigt}} &= \frac{1}{9}(2C_{11}+C_{33}) + \frac{2}{9}(C_{12}+C_{13}),\\
G_{\mathrm{Hill}} &= \frac{1}{2}(G_{\mathrm{Reuss}} + G_{\mathrm{Voigt}}),\\
G_{\mathrm{Reuss}} &= 15[4(2S_{11}+S_{33}) - 4(S_{12}+2S_{13})\\
&\quad + 6(S_{44}+S_{11}-S_{12})]^{-1},\\
G_{\mathrm{Voigt}} &= \frac{1}{15}(2C_{11}+C_{33}-C_{12}-2C_{13})\\
&\quad + \frac{1}{5}\left(2C_{44} + \frac{C_{11}-C_{12}}{2}\right).
\end{aligned} \tag{7}$$

The Young's modulus E and Poisson coefficient v are related to the hardness for polycrystalline material. These quantities are given by [34]:

$$E_X = \frac{9B_X G_X}{G_X + 3B_X}\,,$$
$$v = \frac{1}{2}\left[\frac{B_X - (2/3)G_X}{B_X + (1/3)G_X}\right], \tag{8}$$

where X is Voigt, Reuss or Hill, and S_{ij} is the inverse matrix of the elastic constants matrix C_{ij}, which is given by [35]

$$\begin{aligned} S_{11} &= (C_{11}C_{33} - C_{13}^2)/ \\ &\quad [(C_{11} - C_{12})(C_{11}C_{33} + C_{12}C_{33} - 2C_{13}^2)\,, \\ S_{12} &= (C_{13}^2 - C_{12}C_{33})/ \\ &\quad [(C_{11} - C_{12})(C_{11}C_{33} + C_{12}C_{33} - 2C_{13}^2)\,, \\ S_{13} &= -C_{13}/(C_{11}C_{33} + C_{12}C_{33} - 2C_{13}^2)\,, \\ S_{33} &= (C_{11} + C_{12})/(C_{11}C_{33} + C_{12}C_{33} - 2C_{13}^2)\,, \\ S_{44} &= 1/C_{44}\,. \end{aligned} \tag{9}$$

Moreover, the elastic anisotropy ratio is an important physical quantity about the structural phase stability of crystal structures and the anisotropies of the compressional (P) and two shear waves (S_1 and S_2) which are defined as [36]

$$\Delta p = \frac{C_{33}}{C_{11}}\,,$$
$$\Delta s_1 = \frac{C_{11} - C_{13}}{2C_{44}}\,,\quad \Delta s_2 = \frac{2C_{44}}{C_{11} - C_{12}}\,. \tag{10}$$

3. Results and Discussion

3.1. Structure and Equation of States

CaN_2, BaN_2, and SrN_2 have previously been synthesized and carefully characterized [9, 12 – 14, 23, 37]. CaN_2 (space group $I4/mmm$ (no. 139), $a = 3.5747$ Å, $c = 5.9844$ Å, $Z = 2$ where calcium and nitrogen atoms occupy the 2a and 4e Wyckoff positions with $w_{Rp} = 0.078$), SrN_2 (space group $I4/mmm$ (no. 139), $a = 3.8054$ Å, $c = 6.89614$ Å, $Z = 2$ where stron-

Table 1. Lists the obtained structural parameters lattice constant a, b, c (in Å) for CaN_2, SrN_2, and BaN_2 at zero pressure and zero temperature, together with the experimental and other theoretical values.

Species	This work	Methods	PSP	a (Å)	b (Å)	c (Å)	β (°)
CaN_2		GGA PBE	NC	3.6016		5.9342	
		LDA CA-PZ	US	3.6152		5.9373	
			OTF	3.6153		5.9360	
			NC	3.7156		5.9970	
			US	3.6936		6.0598	
			OTF	3.6741		6.1157	
	Exp. [23]			3.5747		5.9844	
SrN_2		GGA PBE	NC	3.8058		6.8916	
		LDA CA-PZ	US	3.8242		6.7059	
			OTF	3.8266		6.7378	
			NC	3.8445		6.4123	
			US	3.5454		6.3431	
			OTF	3.8356		6.4758	
	Cal. [12]			3.8054		6.8961	
	Exp. [23, 38]			3.8054		6.8961	
				3.8136		6.2155	
BaN_2		GGA PBE	NC	7.1738	4.3715	7.1802	104.9156
		LDA CA-PZ	US	7.0500	4.4648	7.3258	104.2591
			OTF	7.2013	4.4478	7.2993	104.4585
			NC	7.0462	4.3771	7.1765	104.3827
			US	6.9802	4.3784	7.1134	104.0835
			OTF	6.9545	4.3704	7.0844	104.0533
	Cal. [13]			7.1608	4.3776	7.2188	104.9679
	Exp. [23, 38]			7.1608	4.3776	7.2188	104.9679
				7.1712	4.3946	7.2393	104.8641

tium and nitrogen atoms occupy the 2a and 4e Wyckoff positions with $w_{Rp} = 0.057$), and BaN_2 (space group $C2/c$ (no. 15) with $a = 7.1604$ Å, $b = 4.3776$ Å, $c = 7.2188$ Å, $\beta = 104.9679°$, $Z = 4$ where barium and nitrogen occupy the 4e and 8f Wyckoff positions with $w_{Rp} = 0.049$) [23, 38] were investigated. We obtained the equilibrium lattice parameters a and c of CaN_2 and SrN_2, and the a, b, c, and β values of BaN_2 using total energy calculations. The obtained lattice constants and the GGA as well as LDA calculations at 0 GPa and 0 K are summarized in Table 1 together with the available experimental and theoretical results for comparison.

The lattice constants a for GGA-NC, GGA-US, GGA-OTF, LDA-NC, LDA-US, and LDA-OTF are slightly higher than the experimental value (3.5447 Å) [23] with errors of (0.752%, 1.133%, and 1.136% for GGA-NC, GGA-US, and GGA-OTF, respectively, and 3.941%, 3.326%, and 2.782% for LDA-NC, LDA-US, and LDA-OTF, respectively). The lattice constants c for GGA-NC, GGA-US, and GGA-OTF are slightly lower than the experimental value (5.9844 Å) with errors of 0.781%, 0.839%, and 0.809% for GGA-NC, GGA-US, and GGA-OTF, respectively, and those for LDA-NC, LDA-US, and LDA-OTF are slightly higher compared with the experimental values with errors of 2.10%, 1.23%, and 2.14% for LDA-NC, LDA-US, and LDA-OTF, respectively. Furthermore, we compared the lattice constants of SrN_2 and BaN_2 with the experimental values [12, 13]. The results for the GGA and LDA of CaN_2, SrN_2, and BaN_2 are reasonable when compared with experimental values. The obtained lattice parameters for GGA-NC are most consistent with the experimental results. We thus used GGA-NC for the following calculations.

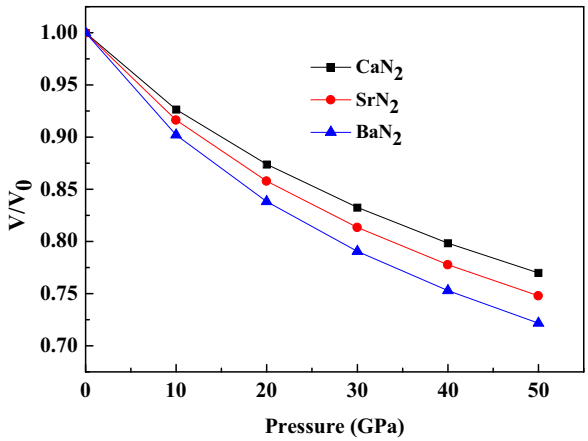

Fig. 1 (colour online). Normalized volume V_n ($V_n = V/V_0$, V_0 is our calculated equilibrium volume at zero pressure) dependence of the resulting pressure P of CaN_2, SrN_2, and BaN_2.

By fitting the calculated E–V data to the Vinet EOS, the bulk modulus B_0 at $P = 0$ and $T = 0$ can be obtained. The obtained values for $CaN_2(B_0 = 111.32\,\text{GPa})$, $SrN_2(B_0 = 96.08\,\text{GPa})$, and $BaN_2(B_0 = 96.08\,\text{GPa})$ indicate that the hardness decreases from CaN_2 to BaN_2. These values are much larger than the theoretical values: $CaN_2(B_0 = 77\,\text{GPa})$, $SrN_2(B_0 = 65\,\text{GPa})$, and $BaN_2(B_0 = 46\,\text{GPa})$ [39]. Deviations from previous theoretical data of GGA are 44.45%, 47.81%, and 71.36%, respectively. The significant difference might come from the approximation used in the calculation method. Each calculation method has its own limitations because of the basic material parameter basis sets and the precision used. The pressure derivatives B_0' for $CaN_2(B_0' = 4.407\,\text{GPa})$, $SrN_2(B_0' = 3.96\,\text{GPa})$, and $BaN_2(B_0' = 4.17\,\text{GPa})$ are slightly different to the theoretical values: $CaN_2(B_0' = 4.12\,\text{GPa})$, $SrN_2(B_0' = 4.47\,\text{GPa})$, and $BaN_2(B_0' = 4.78\,\text{GPa})$ [39].

The crystal volumes V of GGA-NC for CaN_2, SrN_2, and BaN_2 were found to be 79.562 Å^3, 92.807 Å^3, and 230.794 Å^3. In Figure 1, we show the normalized volume V_n ($V_n = V/V_0$ where V_0 is the calculated equilibrium volume at zero pressure), which is dependent on the resulting pressure P for CaN_2, SrN_2, and BaN_2. As shown in Figure 1, BaN_2 is more compressible than CaN_2 and SrN_2 as the pressure increases. Figure 2 shows energy–volume curves for CaN_2, SrN_2, and BaN_2, and these were obtained using non-spin polarized (NSP) and spin polarized (SP) calculations. Figure 2 clearly reveals that NSP-CaN_2, NSP-SrN_2, and NSP-BaN_2 are energetically more stable. The pressure dependence of the N–N distance (Å) of CaN_2, SrN_2, and BaN_2 at zero temperature is listed in Table 2. These are compared with the available experimental and theoretical results. The N–N distances for the three metal-diazenides decreased with an increase in pressure, which means that the volume of the three crystal structures decreased significantly. However, the N–N distances of the diazenides at zero pressure are significantly different to the experimental [23] and theoretical [39] data. However, the results are consistent with experimental data for a pressure around 50 GPa [23]. The reason may be the synthesis of metal-diazenides under high pressure.

Pressure (GPa)	CaN_2 N–N dist. (Å)	SrN_2 N–N dist. (Å)	BaN_2 N–N dist. (Å)
0	1.236	1.278	1.245
10	1.232	1.277	1.243
20	1.229	1.268	1.241
30	1.218	1.265	1.238
40	1.215	1.261	1.235
50	1.212	1.257	1.231
Cal. [11, 39]	1.255	1.254	1.230
Exp. [38]	1.202	1.239	1.232

Table 2. Pressure dependence of the N–N distance (Å) of CaN_2, SrN_2, BaN_2 at zero temperature.

3.2. Elastic Properties

Elastic constants provide a link between the mechanical and dynamic behaviour of crystals. Our calculated elastic constants for CaN_2 at zero pressure and zero Kelvin are $C_{11} = 108.37$, $C_{33} = 304.15$, $C_{44} = 19.66$, $C_{12} = 54.75$, and $C_{13} = 34.18$ GPa. For SrN_2, they are $C_{11} = 97.22$, $C_{33} = 267.7$, $C_{44} = 17.73$, $C_{12} = 54.22$, and $C_{13} = 20.33$ GPa. For BaN_2, they are $C_{11} = 70.45$, $C_{33} = 76.59$, $C_{44} = 28.54$, $C_{12} = 39.62$, and $C_{13} = 38.62$ GPa. Unfortunately, no data exist for comparison. In Figure 2, the pressure dependence of the elastic con-

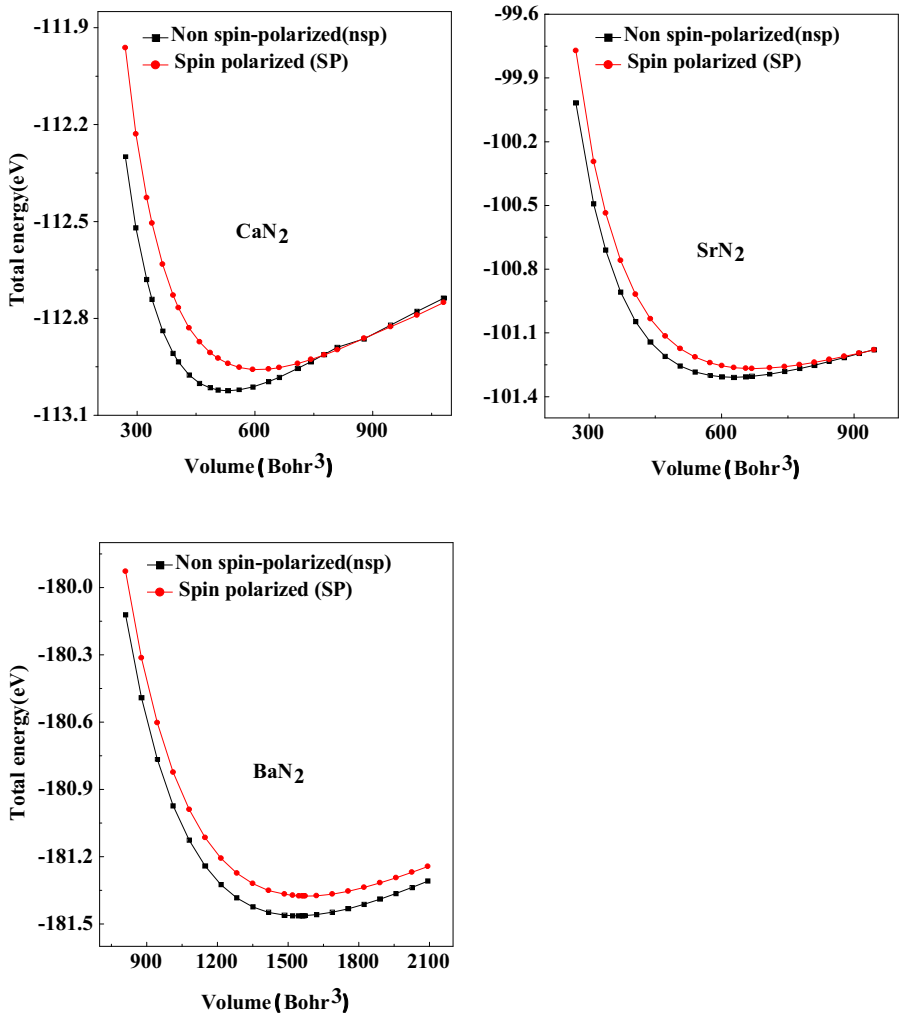

Fig. 2 (colour online). Theoretically obtained total energy as a function of volume for both spin polarized and non-spin polarized CaN_2, SrN_2, and BaN_2.

stants of CaN_2, SrN_2, and BaN_2 at zero temperature and at different pressures is shown. C_{11}, C_{33}, C_{12}, C_{13} for CaN_2, SrN_2, and BaN_2 increase constantly with an increase in pressure; however, C_{44} for CaN_2, and SrN_2 decreases with a change in pressure. The C_{44} for BaN_2 is different as shown in Figure 2, as it increases with an increase in pressure. Additionally, $C_{33} > C_{11}$ implies that the atomic bonds along the {0 0 1} planes between the nearest neighbours are stronger than those along the {1 0 0} planes. For CaN_2 and SrN_2 the applied pressures increase this difference. However, for BaN_2, C_{33}, and C_{11} have approximate values, which shows that the atomic bonds along the {0 0 1} planes between nearest neighbours are similar to those along the {1 0 0} plane.

We studied the mechanical stability of CaN_2, SrN_2, and BaN_2 using mechanical stability criteria. According to Sin'ko and Smirnov's conditions of mechanical stability [40], mechanical stability should conform to the following conditions:

$$\tilde{C}_{44} > 0\,,\ \tilde{C}_{11} > \left|C'_{12}\right|,$$
$$\tilde{C}_{33}(\tilde{C}_{11}+\tilde{C}_{12}) > 2\tilde{C}_{13}^2\,,$$

where $\tilde{C}_{\alpha\alpha} = C_{\alpha\alpha} - P(\alpha = 1,3,4)$, $\tilde{C}_{12} = C_{12} + P$, $\tilde{C}_{13} = C_{13} + P$. The mechanical stability of CaN_2, SrN_2, and BaN_2 was plotted as a function of pressure in Figure 3. When one of the above-mentioned conditions is no longer fulfilled, the compound is not mechanically stable. In Figure 3, the critical pressure was ~20 GPa for CaN_2, ~15 GPa for SrN_2, and ~10 GPa for BaN_2. We also found that when the pressure reached 50 GPa, the mechanical stability conditions were fulfilled. Kulkarni et al. [9] obtained a CaC_2-I-type structure ($I4/mmm$ no. 139) and a CaC_2-V-type structure ($Immm$ no. 77) for CaN_2 using the global energy landscape and subsequent local optimization, respectively. The CaC_2-V-type structure of CaN_2 is formed upon an increase in pressure. This is consistent with our conclusions for a pressure up to 20 GPa where the mechanical stability was disrupted. Furthermore, BaN_2 has an analogous structure to ThC_2 and CaN_2-I. The CaN_2-I structure is metastable to at least 20 GPa and SrN_2 crystallizes as a CaC_2-I-type structure under standard pressure while a tetragonal CaC_2-I-type structure exists under high pressure [9].

The calculated bulk, shear, and Young's moduli as well as the Poisson coefficient are summarized in Table 3. From our values, the B_x/C_x for CaN_2, SrN_2, and

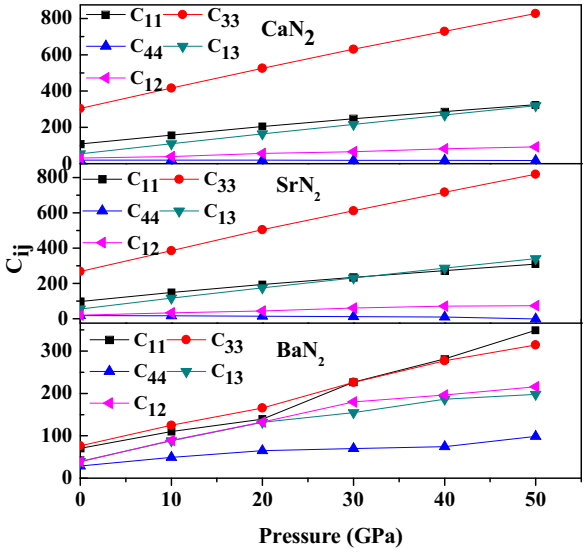

Fig. 3 (colour online). Pressure dependence of the elastic constants of CaN_2, SrN_2, and BaN_2 at zero temperature.

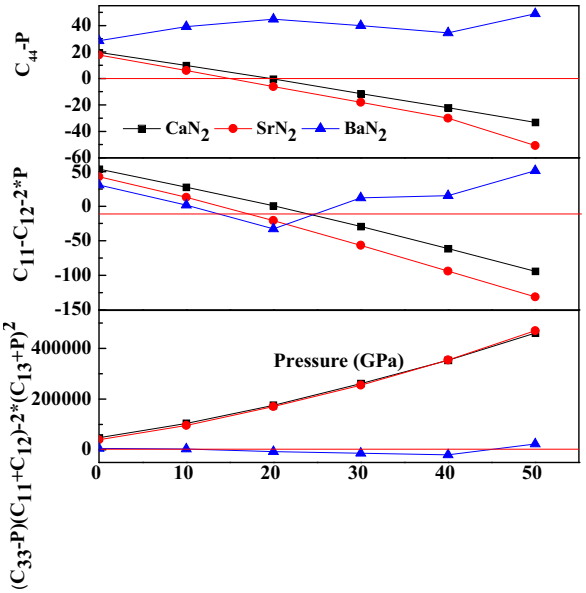

Fig. 4 (colour online). Mechanical stability versus pressure of CaN_2, SrN_2, and BaN_2.

BaN_2 indicates that the parameter limiting the stability of this compound is the shear modulus. Additionally, the lower Poisson coefficients for CaN_2, SrN_2, and BaN_2 mean that an increase in the volume is associated with uniaxial tensile deformation. According to the criterion of Pugh [41], if the B_x/G_x parameter, defined as

the shear modulus relative to the resistance to fracturing, is higher than 1.75, the material should be ductile. For our metal–nitrogen compounds, the B_x/G_x values are all more than 1.75, which means that those compounds will behave in a ductile manner. Additionally, the elastic anisotropy ratio is an important physical parameter for the structural phase stability of crystal structures. The anisotropy ratios of the three metal–nitrogen compounds were estimated and indicated anisotropy. Moreover, for an anisotropic system, small C_{13}/C_{12} and large C_{33}/C_{11} values indicate that atomic bonding along the z-axis is stronger than along the x-axis for CaN_2, SrN_2, and BaN_2.

3.3. Electronic Structure

The electronic structures of CaN_2, SrN_2, and BaN_2 have been investigated previously [12, 13, 23, 37]. Our electronic structure calculations predict a density of states (DOS) with metallic behaviour, which is in good agreement with that of previous studies [23, 37]. The same energetic sequence is shown in the bands in Figures 5 and 6 but minor differences exist in terms of the location of the band centers and the dispersion. The band structure of CaN_2 along the selected high symmetry lines within the first Brillouin zone as well as the partial DOS of all three compounds are shown in Figures 5 and 6. In these figures, four groups of bands are identified. The two low-energy groups of bands each comprise four single bands. The bands are most easily counted along the N-R line where they are fourfold degenerate. The bonding states at about −20 eV are mainly based on the dumbbell. At about −10 eV,

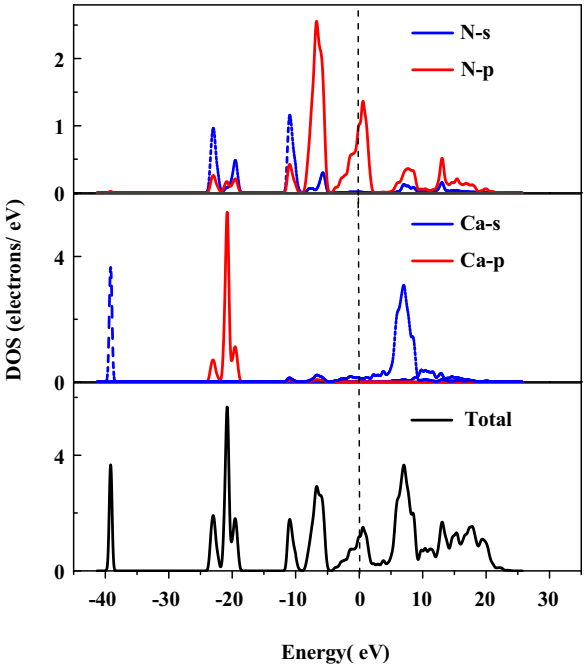

Fig. 5 (colour online). Total and partial density of states of CaN_2.

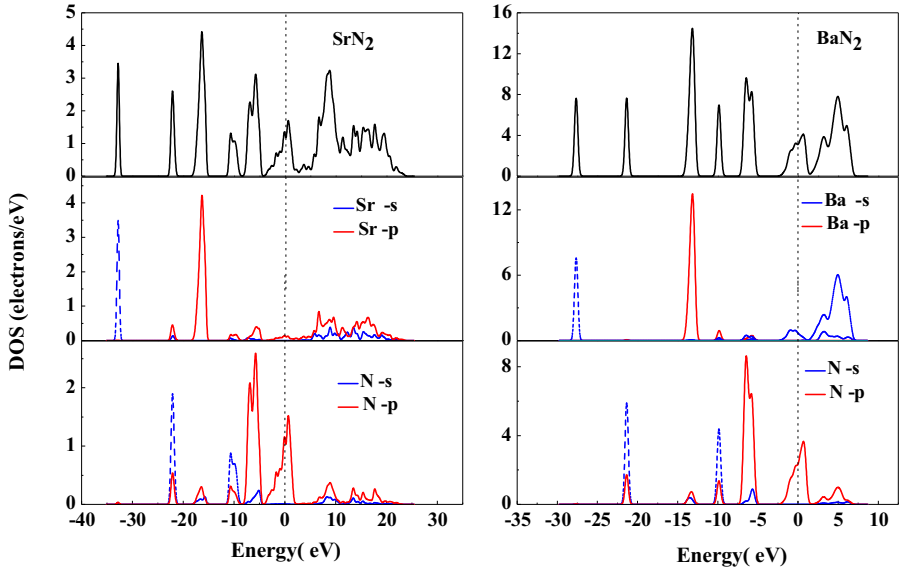

Fig. 6 (colour online). Total and partial density of states of SrN_2 and BaN_2.

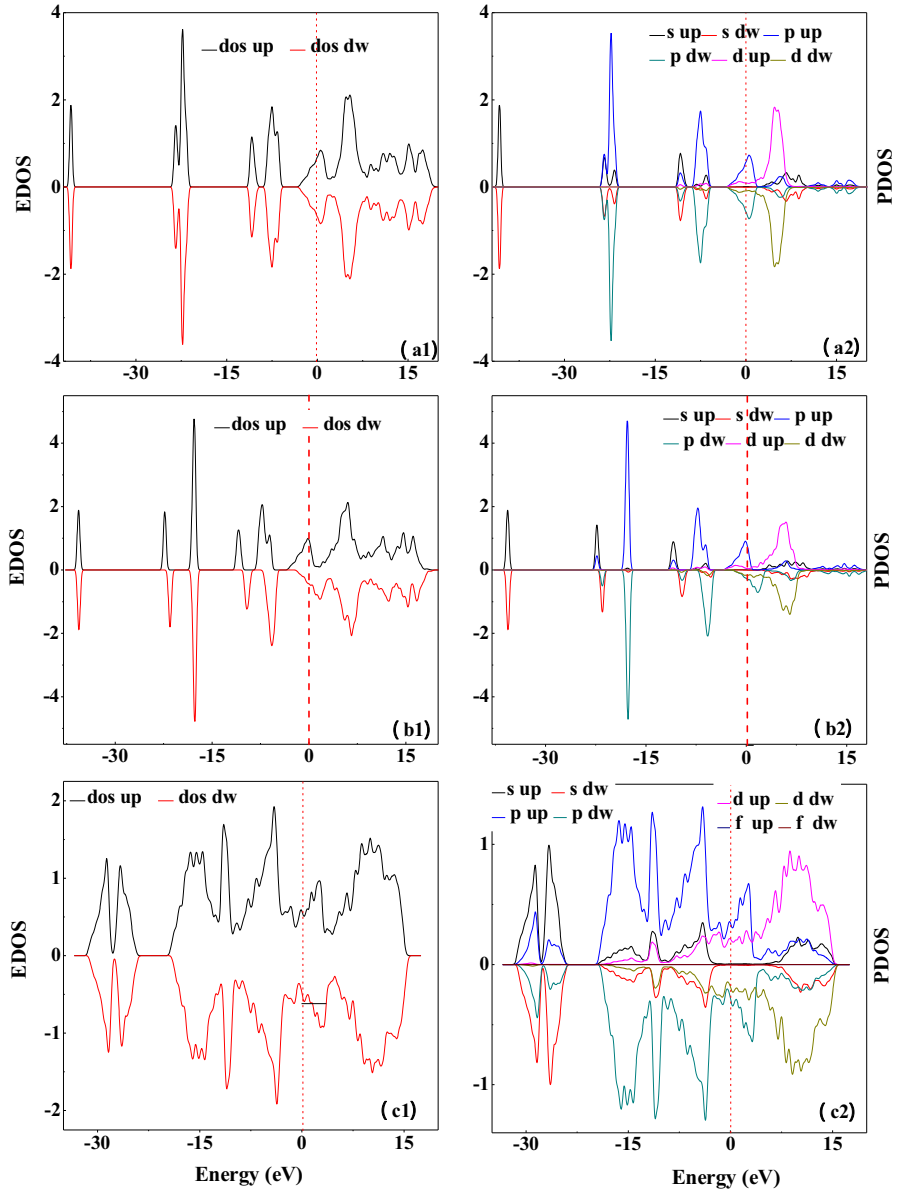

Fig. 7 (colour online). (a1) Total electronic density of states and (a2) the projected electronic densities of states of CaN_2 for spin-up and spin-down case. (b1) Total electronic density of states and (b2) the projected electronic densities of states of SrN_2 for spin-up and spin-down case. (c1) Total electronic density of states and (c2) the projected electronic densities of states of BaN_2 for spin-up and spin-down case.

the dinitrogen states mix with $3s/4p$ Ca, $4s/5p$ Sr, and $5p/6s$ Ba. The antibonding bands in the proximity of the Fermi level that ranges from -5 to 3 eV are basically built up by the π^* states of the dinitrogen unit, which is slightly mixed with the $3s/4p$ Ca, $4s/5p$ Sr, and $5p/6s$ Ba. The bands above 3 eV are predominantly formed by $3s/4p$ Ca, $4s/5p$ Sr, and $5p/6s$ Ba. The itinerant electrons in the N-dominated region are the carriers of electrons in the N-dominated region. From CaN_2 to SrN_2 to BaN_2 the increase in ionicity is clear as shown by an increase in the sharpness of the nitrogen π states, which parallels the difference in Pauling electronegativities ($\Delta EN(M-N) = 1.4, 1.7, 2.0$) between the alkaline-earth metals and nitrogen in this series [23, 39].

A discussion about the magnetic properties of the MN_2(M = Ca, Sr, Ba) compounds is warranted. The spin polarized equilibrium lattice constants for the sug-

Table 3. Calculated bulk, shear, and Young's modulus (in GPa), B_x/G_x, Poisson coefficient and the anisotropies of the compressional (P) and two shear waves (S_1 and S_2).

	B_X (GPa)			G_x (GPa)			B_x/G_x		
	B_R	B_V	B_H	G_R	G_V	G_H	X = R	X = V	X = H
CaN_2	83.91	73.71	78.81	45.54	26.90	37.37	1.86	2.45	2.11
SrN_2	72.53	65.73	69.13	41.12	26.10	33.61	1.76	2.52	2.07
BaN_2	48.52	48.14	48.33	27.47	20.01	23.74	1.77	2.40	2.03
	E_x (GPa)			v_X			Anisotropy		
	E_R	E_V	E_H	v_R	v_V	v_H	Δ_p	Δ_{s1}	Δ_{s2}
CaN_2	114.83	78.33	96.81	0.27	0.32	0.29	2.81	1.89	0.73
SrN_2	144.17	97.99	121.67	0.26	0.32	0.29	2.75	2.17	0.83
BaN_2	69.33	52.72	61.19	0.26	0.32	0.29	1.08	1.85	0.56

gested structures of CaN_2, SrN_2, and BaN_2 were obtained upon geometry optimization as: $a = 3.658$, $c = 5.992$ Å; $a = 3.838$, $c = 6.902$ Å; and $a = 7.221$, $b = 4.477$, $c = 7.347$, and $\beta = 104.367°$, respectively. Additionally, we found that the total spin magnetic moments are: 1.049 μ_B, 1.059 μ_B, and 1.014 μ_B, respectively. From Figure 7a–c we conclude that the region (−4,0), (−5,0), and (−10,0) may be viewed as bonding states while the unoccupied higher region corresponds to anti-bonding states between the (0,8), (0,8), and (0,15) N-2p and N-2p states. From the high EDOS, a Stoner instability exists at the spin polarized equilibrium for the three diazenide compounds.

4. Conclusion

In summary, we performed first-principles non-spin and spin polarized computations on alkaline earth diazenides and determined various structural parameters and their elastic, electronic, and bonding behaviour. The structural parameters obtained after relaxation are similar to those in previous reports. We calculated the elastic constants and derived the bulk and shear moduli, Young's modulus and the Poisson coefficient. The results show that the alkaline earth diazenides are mechanically stable and behave in a ductile manner at zero pressure. The bulk modulus calculations confirmed that the hardness decreases from CaN_2 to SrN_2 to BaN_2. As the applied pressure increases, our calculations predict mechanical instabilities at 20, 15, and 10 GPa for CaN_2, SrN_2, and BaN_2, respectively. The density of states suggest a metallic nature and hint at the role of electrons near the Fermi level in establishing the directional bonding between Ca-p, Sr-p, Ba-p, and N-p states and the electronic stability of the alkaline earth diazenides.

[1] A. F. Young, C. Sanloup, E. Gregoryanz, S. Scandolo, R. J. Hemley, and H. K. Mao, Phys. Rev. Lett. **96**, 155501 (2006).

[2] Z. W. Chen, X. J. Guo, Z. Y. Liu, M. Z. Ma, Q. Jing, G. Li, X. Y. Zhang, L. X. Li, Q. Wang, Y. L. Tian, and R. P. Liu, Phys. Rev. B **75**, 103 (2007).

[3] J. A. Montoya, A. D. Hernandez, C. Sanloup, E. Gregoryanz, and S. Scandolo, Appl. Phys. Lett. **90**, 011909 (2007).

[4] J. C. Crowhurst, A. F. Goncharov, B. Sadigh, C. L. Evans, P. G. Morrall, J. L. Ferreira, and A. G. Nelson, Science **311**, 1275 (2006).

[5] A. Yildiz, Ü. Akinci, O. Gülseren, and İ. Sökmen, J. Phys. Condens. Matter **21**, 403 (2009).

[6] C. Jiang, Z. Lin, and Y. Zhao, Phys. Rev. Lett **103**, 185501 (2009).

[7] Y. Liang, J. Zhao, and B. Zhang, Solid State Commun. **146**, 450 (2008).

[8] Y. Li and Y. Ma, Solid State Commun. **150**, 759 (2010).

[9] A. Kulkarni, J. C. Schön, K. Doll, and M. Jansen, Chem. Asian J. **8**, 743 (2013).

[10] J. von Appen, M.-W. Lumey, and R. Dronskowski, Angew. Chem. Int. Ed. **45**, 4365 2006.

[11] F. Bachhuber, J. Rothballer, F. Pielnhofer, and R. Weihrich, J. Chem. Phys. **2011**, 135 124508.

[12] G. Auffermann, Y. Prots, and R. Kniep, Angew. Chem. Int. Ed. **40**, 547 (2002).

[13] G. Auffermann, U. Schmidt, B. Bayer, Y. Prots, W. Schelle. R. K. Kremer, A. Simon, and R. Kniep, Inorg. Chem. **40**, 4866 (2001).

[14] G. V. Vajenine, G. Auffermann, Y. Ports, R. Kniep, and W. Bronger, Z. Anorg. Allg. Chem. **632**, 565 (2006).

[15] E. Gregoryanz, C. Sanloup, M. Somayazulu, J. Badro, G. Fiquet, H. K. Mao, and R. J. Hemely, Nat. Mater. **3**, 294 (2004).

[16] J. V. Appen, M. W. Lumey, and R. Dronskowski, Angew. Chem. **118**, 4472 (2006).
[17] J. C. Crowhurst, A. F. Goncharov, B. Sadigh, C. L. Evans, P. G. Morrall, J. L. Fereira, and A. J. Nelson, Science **311**, 1275 (2006).
[18] A. F. Young, J. A. Montoya, C. Sanloup, M. Lazzeri, E. Gregoryanz, and S. Scandolo, Phys. Rev. B **73**, 153102 (2006).
[19] J. A. Montoya, A. D. Hernández, C. Sanloup, E. Gregoryanz, and S. Scandolo, Appl. Phys. Lett. **90**, 011909 (2007).
[20] Z. W. Chen, X. J. Guo, Z. Y. Liu, M. Z. Ma, Q. Jing, G. Li, X. Y. Zhang, L. X. Li, Q. Wang, Y. J. Tian, and R. P. Liu, Phys. Rev. B **75**, 054103 (2007).
[21] W. Chen, J. S. Tee, and J. Z. Jiang, Phys. Condens. Matter **22**, 015404 (2010).
[22] R. Yu, Q. Zhan, and L.C. De Jonghe, Angew. Chem. Int. Edit. **46**, 1136 (2007).
[23] S. B. Schneidern, R. Frankovsky, and W. Schnick, Inorg. Chem. **51**, 2366 (2012).
[24] M. D. Segall, P. J. D. Lindan, M. J. Probert, C. J. Pickard, P. J. Hasnip, S. J. Clark, and M. C. Payne, J. Phys. Condens. Matter **14**, 2717 (2002).
[25] S. H. Vosko, L. Wilk, and M. Nusair, Can. J. Phys. **58**, 1200 (1980).
[26] J. P. Perdew, K. Burke, and M. Ernzerhof, Phys. Rev. Lett. **77**, 3865 (1996).
[27] H. J. Monkhorst and J. D. Pack, Phys. Rev. B **13**, 5188 (1976).
[28] P. Vinet, J. H. Rose, J. Ferrante, and J. R. Smith, J. Phys. Condens. Matter **1**, 1941 (1989).
[29] D. C. Wallace, Thermodynamics of Crystals, Wiley, New York 1972.
[30] B. B. Karki, G. J. Ackland, and J. Crain, J. Phys. Condens. Matter **9**, 8579 (1997).
[31] W. Voigt, Lehrbuch der Kristallphysik, Teubner, Leipzip 1928.
[32] A. Ruess, Z. Angew. Math. Mech. **9**, 49 (1929).
[33] R. Hill, Proc. Soc. London. A **65**, 349 (1952).
[34] E. Schreiber, O. L. Anderson, and M. Saga, Elastic Constants and Their Measurement, McGraw-Hill, New York, 1973.
[35] H. S. Chen, Anisotropy of Elasticity About Metal, Metallurgy Industry Press, Beijing 1996.
[36] X. H. Deng, W. Lu, Y. M. Hu, and H. S. Gu, Physica B **404**, 1218 (2009).
[37] S. B. Schneider, M. Mangstl, G. M. Friederichs, R. Frankovsky, J. S auf der Günne, and W. Schnick, Chem. Mater. **25**, 4149 (2013).
[38] S. B. Schneider, R. Frankovsky, and W. Schnick, Angew. Chem. **124**, 1909 (2012).
[39] M. Wessel and R. Dronskowski, J. Comp. Chem. **31**, 1613 (2010).
[40] G.V. Sin'ko and N. A. Smirnov, J. Phys. Condens. Matter **14**, 6989 (2002).
[41] S. F. Pugh, Philos. Mag. **45**, 833 (1954).